Manifestation of intrinsic defects in optical properties of self-organized opal photonic crystals

Yu. A. Vlasov,* V. N. Astratov,† A. V. Baryshev, A. A. Kaplyanskii, O. Z. Karimov,‡ and M. F. Limonov
A. F. Ioffe Physical-Technical Institute, 194021, St. Petersburg, Russia
(Received 19 August 1999)

Self-organized synthetic opals possessing a face centered cubic (fcc) lattice are promising for fabrication of a three-dimensional photonic crystal with a full photonic band gap in the visible. The fundamental limiting factor of this method is the large concentration of lattice defects and, especially, planar stacking faults, which are intrinsic to self-assembling growth of colloidal crystal. We have studied the influence of various types of defects on photonic band structure of synthetic opals by means of optical transmission, reflection and diffraction along different crystallographic directions. We found that in carefully chosen samples the stacking probability α can be as high as 0.8–0.9 revealing the strong preference of fcc packing sequence over the hexagonal close-packed (hcp). It is shown that scattering on plane stacking faults located perpendicular to the direction of growth results in a strong anisotropy of diffraction pattern as well as in appearance of a pronounced doublet structure in transmission and reflection spectra taken from the directions other than the direction of growth. This doublet is a direct manifestation of the coexistence of two crystallographic phases—pure *fcc* and strongly faulted. As a result the inhomogeneously broadened stop-bands overlap over a considerable amount of phase space. The latter, however, does not mean the depletion of the photonic density of states since large disordering results in filling of the partial gaps with both localized and extended states.

PACS number(s): 42.70.Qs, 82.70.Dd, 61.72.Nn, 42.25.Bs

I. INTRODUCTION

Significant attention has been paid recently to various routes for fabrication of artificial dielectric microstructures called ''photonic crystals'' [1]. These materials consist of a periodic repetition of dielectric elements (''atoms'' of the structure) in analogy to the way atoms form the lattice of usual solids. Light with a wavelength close to the period of the photonic crystal will bounce between these ''atoms,'' interfere and totally reflect back. Light of other colors will pass through. Such selective filtering is known as a ''photonic band gap'' (PBG)—the range of wavelengths, which cannot propagate through the photonic crystal due to interference. Although the initial ideas were introduced more than a decade ago, the experimental studies of optics of photonic crystals, which are important for both fundamental and applied physics are, however, still at the beginning. This is dictated mainly by serious difficulties encountered by today's technology in production of the three-dimensionally periodic solid with the ''atom'' size of the order of the wavelength of visible light.

Self-organization of spherical colloidal microparticles has been proposed as a possible route to create PBG crystals [2–14]. As in a natural gemstone opal [15], such artificial structures are formed from submicron glass or polymer marbles self-assembled during sedimentation onto a face centered cubic (fcc) lattice. Relatively low refractive index contrast of the bare opal does not allow large perturbations of the photonic density of states (DOS) [4] necessary for opening of an omnidirectional PBG. Fortunately the material is shown to be technologically very flexible. It is feasible to increase the refractive index contrast in opals by filling of the interstitials with a semiconductor material [7,16,17] or by making opals from semiconducting spheres [18]. The possibility to vary the volume packing fraction of the spheres β in opal lattice from $\beta=0.74$ to unity by controllable sintering [5,19] complement this list.

Initial estimations [5,7] have shown that photonic ''pseudogap'' (strong depletion of photonic DOS between the lowest lying zones in fcc lattice [20]) or higher order complete omnidirectional photonic band gap [21] can be achieved in opals with ''air-spheres'' type of lattice, when the refractive index of the spheres n_a is much smaller than refractive index of interstitials n_b. The required parameters for opening of PBG were estimated as $n_b/n_a=2.5$ and $\beta=0.86$ larger than the close-packed value. Further rigorous theoretical calculations confirm that omnidirectional PBG indeed opens in such ''inverted opals'' for similar parameters [22,23] ($n_a/n_b=2.85$ for $\beta=0.74$ with a tendency of increase of the gap size with increasing β).

These predictions stimulate intense recent experimental studies of various routes for fabricating of ''inverted opals.'' The periodic opal lattice is used as a scaffolding for high refractive index materials like titanium dioxide [24], graphite [25], or semiconductor quantum dots [26]. After removing the microspheres from the structure the refractive index contrast can be increased to values high enough for opening up a complete photonic band gap. Thus it has been shown that self-assembly of colloidal microspheres, being very cheap and relatively easy method, can successfully compete with more sophisticated methods of production of photonic band gap crystals for visible wavelengths, like reported recently micromachining of a 3D crystal of silicon logs [27].

The method of self-organization, however, possesses several intrinsic difficulties, which can significantly narrow its

*Author to whom correspondence should be addressed. Present address: NEC Research Institute, 4 Independence Way, Princeton, NJ 08540. URL:www.neci.nj.nec.com/homepages/vlasov

†Present address: Department of Physics and Astronomy, University of Sheffield, Sheffield S3 7RH, UK.

‡Present address: Department of Physics, University of Bath, Bath BA2 7AY, UK.

applicability. One of the fundamental limiting factor of this method is the large concentration of various type of defects, which are intrinsic to self-assembling growth of colloidal crystal. Indeed, as it was shown theoretically for the simplest model of hard noninteracting spheres [28,29], the thermodynamically stable crystalline phase appears to be fcc. The free energy difference between hexagonal close packed structure (hcp) and fcc is found, however, to be only about $10^{-3}k_B$ per sphere [28–30]. This results in generation of a large number of plane stacking faults, which can be characterized by a stacking probability α. For a hcp structure with $ABAB\cdots$ sequence of the close-packed layers $\alpha=0$. For a fcc structure with $ABCABC\cdots$ sequence $\alpha=1$. Stacking faults are usually generated in a plane of growth and are characterized by a random error in a layers sequence such as $ABCABABC\cdots$ and intermediate values of α. Early studies of natural opals [15], as well as more recent studies of concentrated dispersions [31,32], indicate that the most common type of structures belong to random hexagonally closed packed (rhcp) with $\alpha=0.5$, although some rear samples exhibit purely fcc packing [15]. Studies of colloid crystallization in microgravity conditions reveal the significant role of gravity as a driving force toward the fcc structure [33]. The analysis of light diffraction patterns of sedimented colloidal crystals also reveal the tendency towards fcc with α rising up to 0.8 with the increase of the time of crystallization [31,34]. Recent calculations [35] confirm the possibility of spontaneous transformation of millimeter-sized rhcp to fcc structure on a time scale of months.

In view of above it is not surprising that sedimented colloidal crystals obtained in different laboratories, exhibit strikingly different optical properties. Generally speaking the situation in the field seems to be very analogous to the early days of the physics of semiconductors, with which photonic crystals are most commonly being compared. As is known the early studies of semiconductors were retarded by the extreme sensitivity of the electronic and optical properties to sample-dependent concentrations of impurities and defects. The semiconductors were viewed as a family of solids with irreproducible properties [36]. Efforts of several generations of scientists transform this difficulties into very successful technology of controllable doping. Here we present the first attempt to study the influence of various types of defects of photonic lattice of opals on their photonic band structure by means of optical transmission, reflection, and diffraction. We show that stacking faults are indeed the most common and unavoidable type of defects in synthetic opals, which strongly affect their optical properties. Therefore it is impossible to draw any conclusions on photonic band gap related effects in opals without careful measurements of the concentration of different types of defects and the knowledge of their influence on optical properties of opal. Analysis of optical data allow us to distinguish the contribution of different type of defects to overall optical response of the opal photonic crystal. It is shown that under favorable conditions synthetic opals crystallize preferentially in a fcc lattice with α up to 0.8–0.9 on average. In the best cases the domain size of such a single three-dimensional (3D) crystallite exceeds the 200 μm scale—large enough to perform optical experiments on a single ''defect-free'' photonic crystal [37].

The paper is organized as follows. Section II describes the growth of the samples and their structural characterization. In Sec. III we present the results of transmission and reflection measurements performed along [111] direction of growth. Section IV describes the transmission and reflection along directions other than [111]. Section V is devoted to the results of diffraction measurements. Finally we come to conclusions in Sec. VI.

II. SAMPLE PREPARATION AND CHARACTERIZATION

A. Growth and preparation of the samples

Most of the samples of synthetic opal used in this study were purchased commercially [38]. Additionally, in order to study the physics of crystal formation we fabricated several samples using well known technological procedure [39], with slight modifications reported by a manufacturer [38]. At first the monodisperse suspensions of SiO_2 spheres with mean diameter d of about 200–400 nm were synthesized by Stöber method [40]. Dynamic light scattering and electron microscopy measurements show that the standard deviation δ of the spheres diameter can be made as low as 2–3 % for each suspension. After synthesis the spheres were resuspended in DI water and the suspension was left undisturbed in a cuvette for a prolonged period (usually about several months). The volume fraction of the spheres in the suspension in sedimentation experiments was much lower than 50%—the critical value reported for freezing transition [41]. These conditions imply the nearly hard-sphere interaction potential [42]. The spheres sedimented slowly driven by gravity at a velocity defined by a Stokes law and accumulated near the bottom of the cuvette in a dense fan. The Peclet number $\mathrm{Pe}=m_b gR/kT$, where m_b is the buoyant mass of a sphere of radius R, which describe the balance between diffusion and sedimentation, is very small for this conditions, typically about 10^{-5}. Corresponding Stokes velocity of sedimentation is of the order of 10^{-6} cm/sec. The sedimentation of the spheres in a dense fan is estimated to be much slower, velocity being significantly smaller than the rate of one-dimensional crystallization (the latter being of the order of 10^{-7} cm/sec for spheres with diameter 200–400 nm [43]). Under these conditions the spheres settling down onto a flat quartz substrate are self-organize in a three-dimensionally periodic structure [43]. Finally the ordered sediment is annealed at hydrothermal conditions in closed volume to provide hardness and to obtain self-supporting solid samples with dimensions in a cm range [39].

The lattice parameter in the crystalline sediment is of the order of the wavelength of visible light. Therefore the dried and annealed samples grown under the conditions described above possess bright iridescence with colored grains prolonged along the growth direction. Since the size of various defects of the lattice is larger than the lattice constant, the defect structure can be examined using an optical microscope or even visually. Scattering on the surface roughness as well as on the defects in the bulk of the sample results in a white milky background. Usually the growth direction is perpendicular to hexagonal close-packed layers and can be referred to as [111] in fcc notation ([0001] in hcp). These layers give the brightest color in diffraction at a longest wavelengths possible for a given lattice parameter [15]. The size of iridescent grains as observed in optical microscope

can vary from very tiny to the scale up to a mm range. These grains can be viewed as individual crystallites with slightly different orientation. This results in different colors seen under some fixed angle to the growth plane. Sometimes the orientation of the grains is correlated to produce a single color and they can be regarded as a domains within a single large crystal. Although the standard deviation of the silica spheres used for opal synthesis is usually below 5%, the slow sedimentation leads to further size separation of the spheres. The lowest layers are composed, therefore, of a spheres with a larger diameter than the upper layers. At the edges of the cuvette the strongly faulted structures can be found, which occur as a result of the influence of the cuvette surface. They can be detected under optical microscope as a thick layers of different colors.

In order to minimize the contribution of these visually seen inhomogeneities the initial annealed chunks were cut by a diamond wheel saw on several parallel plates with a base surface perpendicular to growth direction and each plate was carefully examined under optical microscope. In view of above we chose for our experiments the parts of these plates (typically of 10×10 mm lateral dimensions and thickness of 1–2 mm) cut far from the edges of the cuvette, which exhibit single grain color for a given angle to a [111] planes. In what follows we will discuss only such carefully chosen samples.

B. Electron microscopy characterization

Scanning electron microscopy (SEM) was used for direct characterization of photonic lattice of synthetic opals. The SEM images were obtained at Hitachi SEM-2700 microscope operating at 10–15 kV. To avoid charging the samples were coated with a thin metal and/or carbon layer. Figure 1 displays typical SEM images taken from the different faces of one of the sample (sample GR). Typical surface produced by a cleaving of the sample is shown in Fig. 1(a). The cleaved edge exposes several planes of spheres, which can be identified as $[-11-1]$, [001], [011], and [111] surfaces of a fcc crystal. The orientation of the specific directions along each of the plane can be traced for distances as large as 100–200 μm giving the lower limit of the grain size. Top surface of the as-grown sample [see Fig. 1(b)] reveal hexagonal packing characteristic of [111] planes with monolayer step terraces. Analysis of the sphere packing in several terraces reveal $ABCABC\cdots$ sequence of the layers typical for fcc structure. Figure 1(c) presents the image of the sample surface nearly perpendicular to the [111] plane of growth. The pattern of spheres packing is characteristic for the [110] fcc plane.

All these observations allow to describe the sample as a single crystal with a mostly fcc structure in accord with previously published data [5,19]. Close examination, however, reveals numerous defects of the structure. For [111] orientation of the sample the most visible types of defects are vacancies and interstitials similar to that seen in Fig. 1(b). The total in-plane density of such point defects varies in different samples, however, typical value is estimated as about 10^7 cm^{-2} or 1 defect per 100 unit cell.

Among other types of structural defects these are dislocations and plane stacking faults, which are most commonly observed along the directions perpendicular to the direction of growth. The most simple type of stacking fault is a single

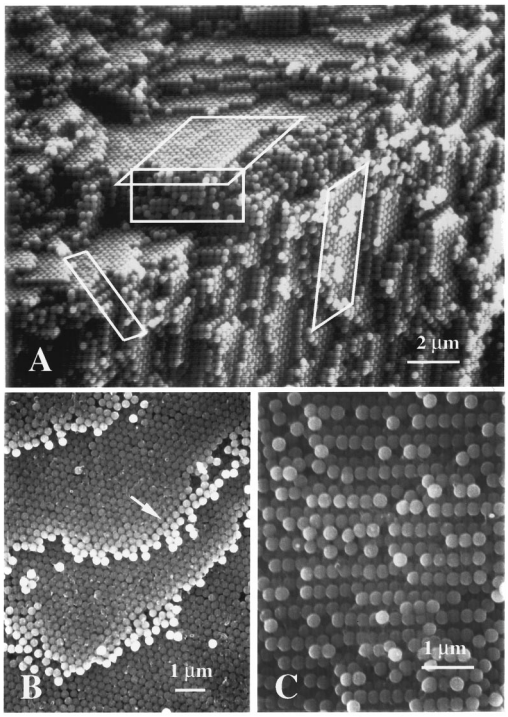

FIG. 1. SEM images of the opal sample GR. (a) Several different planes of a fcc lattice are exposed on the cleaved edge of the sample. (b) Image of the as-grown surface of the sample. Monolayer-step (111) terraces are seen. Arrow shows intrinsic stacking fault. (c) Surface of the (110)-oriented sample.

(or intrinsic [44]) hexagonal triplet of the type $ABCABAABC\cdots$. When viewed on one of the (100) surfaces, this fault give rise to two rows of hexagonal packing in the otherwise square packed plane with a step on the surface along the fault line. Although such defect can also be observed on a (111) growth plane [see arrow in Fig. 1(b)] it does not usually extend over distances larger than few tens of unit cells. In the planes perpendicular to growth direction such defect can extend over several thousands of layers—behavior expected for one-dimensional growth model [43]. More complicated double (or extrinsic) hexagonal triplet ($ABCABACABCABC\cdots$), twinning ($ABCBACBACB\cdots$) or even the whole patch of hexagonal packings form a characteristic pattern of irregular kinks in the (110) plane perpendicular to the (111) growth plane. It has been suggested [45] that calculating the average number of the kinks per unit length can give an estimate of the stacking probability α. We used this method in our samples and found that α strongly depends on the averaging volume. Indeed, the areas can be found along the (110) plane [similar to that presented in Fig. 1(c)], which are absolutely free from such kinks over hundreds of unit cells. The heavily faulted areas can also be easily found, especially in as-grown chunks. As it was mentioned above for optical measurements the parts of the initial chunks, free from these heavily faulted areas were carefully chosen under optical microscope. The SEM measurements of α on such selected samples gives the values up to 0.8–0.9 indicating strong preference of fcc packing.

C. Orientation of the samples

Since the samples chosen in such a way can be regarded as single crystals (although strongly faulted) then it appears

TABLE I. Parameters of the samples used in experiments.

Sample	BL	GR
a (nm)	289	356
β	0.78	0.78
[111] gap (c/a)	0.62	0.64
[110] gap (c/a)	0.68	0.67
[10−10] gap (c/a)	0.60	0.59
[100] gap (c/a)	n/m	0.73

to be possible to define the orientation of their principal crystallographic axis. The only one direction known *a priori* for as-grown samples is the [111] direction of growth. In order to identify the orientation of the principal crystallographic planes relative to the sample faces we use the SEM images obtained from the sample faces perpendicular to each other similar to that presented on Figs. 1(b) and 1(c) for the sample GR. To identify other main crystallographic directions we controlled the orientation of SEM images relative to the faces of the sample. Two different samples obtained in different technological cycles were examined: the sample BL with fcc lattice constant $a=289$ nm, which displays bright blue color and the green sample GR with $a=356$ nm. The structural parameters of the samples determined by electron microscopy are summarized in Table I. After orientation each of the sample was sawed into three smaller pieces with (111), (110), and (100) orientation of the base plane. The error of the orientation of the base planes lies within $\pm 5°$ interval defined by uncertainty of the cut direction.

III. REFLECTION AND TRANSMISSION ALONG THE [111] DIRECTION OF GROWTH

The transmission spectra were measured using a setup described in detail elsewhere [7,46]. The incident white light beam is produced from an incandescent lamp. In order to minimize the contribution of the spurious diffusely scattered background to the detected signal, the incident beam was highly collimated (divergence less than 200 mrad). The sample is illuminated through a fixed 100 μm diameter diaphragm placed immediately before the sample, thus defining the probing area. To decrease significantly the incoherent scattering on sample surfaces the sample was immersed in a water/glycerin mixture. In this situation the pattern of transmitted light is mainly composed of zero-order ballistically transmitted beam surrounded by a weak diffuse halo. Transmitted light is collected in the direction of incidence within a very narrow angular cone defined by a second diaphragm, which transmits a zero-order beam only. This light is then dispersed with a double, 1.5 m base monochromator (0.5 nm spectral resolution) and recorded by a photomultiplier. Reflection in a nearly backward direction was measured using a small mirror, which limits the smallest incidence angle to about 5 degrees off the normal to the base surface.

Figure 2 summarizes the reflection and transmission spectra taken from the (111) oriented piece cut from the green sample GR. Transmission spectra exhibit the strongly attenuated [111]-photonic gap centered in the vicinity of 557 nm

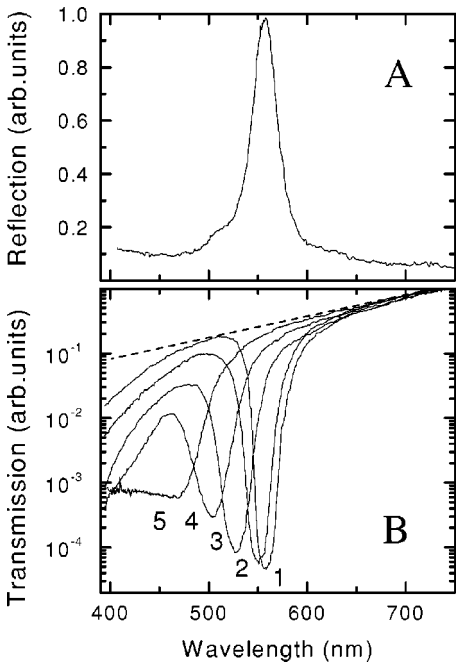

FIG. 2. Reflection (a) and transmission (b) spectra of the [111]-oriented sample GR immersed in glycerin ($n_b=1.47$). The sample thickness is 200 μm. Transmission spectra 1–5 were measured for angles of incidence 0°,20°,30°,40°,54°. The angle is scanned along the L-X direction of fcc BZ. Dotted line shows the Rayleigh scattering contribution.

[spectrum 1 in Fig. 2(b)], which is accompanied with a single intense line in reflection spectrum centered at the same spectral position. The transmission and reflection spectra taken from (111) oriented piece of the sample BL are very similar to that of the sample GR except that the [111]-photonic gap is shifted to the 465 nm because of the smaller lattice constant. The attenuation at the center of the [111] gap is very sensitive to the refractive index of the interstitials n_b, which allows us to determine the refractive index of the spheres n_a by index matching technique [5,7]. For example, the [111] gap practically disappears in transmission spectrum of the sample GR when the sample is immersed in methanol, which corresponds to $n_a \approx n_b \approx 1.32$. For the sample BL the n_a is estimated as 1.37.

To compare spectra obtained on different samples having different lattice constants and different thickness it is useful to present data in some common normalized units. The frequency can be normalized to units of c/a—the speed of light c divided by the fcc lattice constant a. Since attenuation at the frequencies of a [111] photonic gap in synthetic opals depends exponentially on the sample thickness [5,7,46], it can be normalized to units of cm^{-1} of the inverse attenuation length ξ^{-1}, defined as $\xi^{-1}=-\ln(I/I_0)/D$, where D is a sample thickness. Figure 3(a) represents the experimental transmission spectra for both samples GR and BL plotted in normalized units of c/a and ξ^{-1} for the case of $n_b=1.47$. The center of the [111] gap for BL sample corresponds to $\nu=0.62$ with attenuation of 300 cm^{-1}. The [111] gap in the sample GR is shifted to higher frequencies to $\nu=0.64$ and the maximum attenuation is increased to about 470 cm^{-1}, reflecting a decrease of the average refractive index and increase of refractive index contrast.

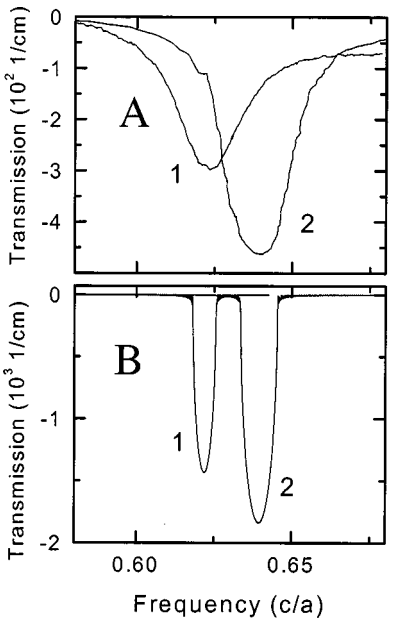

FIG. 3. (a) Transmission spectra of the [111]-oriented samples BL (spectrum 1) and GR (spectrum 2) immersed in glycerin $n_b = 1.47$. The attenuation is corrected for Rayleigh scattering. (b) Calculated transmission spectra for $\langle 111 \rangle$ direction of incidence on the samples with the following parameters $n_a = 1.37$ (line 1) and $n_a = 1.32$ (line 2). Note an order of magnitude difference in the scales of the *y* axis in (A) and (B). Frequency is plotted in normalized units of c/a, where c is a speed of light, a is a lattice constant.

Figure 3(b) represents transmission spectra along the [111] direction in opal photonic lattice calculated using the analytical model [47] based on a simple one-dimensional approach in a scalar wave approximation, which gives qualitatively correct results for the dispersion at high-symmetry points as *X* and, especially, *L* in a fcc Brillouin zone, where a single lattice scattering component dominates. Comparison of Figs. 3(a) and 3(b) reveals that the experimentally observed gap widths are about 5 times larger than calculated. At the same time the calculated attenuation [Fig. 3(b), spectra 1,2] at the center of the gap for both samples BL and GR is roughly an order of magnitude larger than the experimentally measured attenuation of 300 and 470 cm^{-1} [Fig. 3(a), spectra 1,2]. Recently it was argued that such broadening and smoothing of the photonic gap is strongly inhomogeneous in its origin and can lead to light confinement on the structural defects [46]. Consider only one type of defects, which is an unavoidable source of disorder in opal-like self-organized photonic lattices—the deviation δ of the spheres diameters, which in the case under consideration was measured to be about $\delta \approx 5\%$. This results in the same value of the deviation of the lattice constant $a = d\sqrt{2}$. The latter being compared with the calculated normalized width of the [111] stop band $\Delta\lambda/\lambda_0$ in ideal defect-free opal photonic lattice can be the measure of the influence of disorder on the transport properties of photonic crystals [46]. For the present case, as it is seen from calculations presented in Fig. 3(b), the $\Delta\lambda/\lambda_0$ is about 1%. This means that local fluctuations of the photonic band edges are larger than the bandgap width itself, which can result in building up of a strongly confined photonic states [46]. In this condition the edges of the drop in transmission are no longer correspond to the eigenfrequencies of the photonic bands. In practice this implies that the conventional recipe of the experimental determination of the edges of bands as frequencies where the transmission suddenly drops or recovers is no longer valid. Well defined spectral features at frequencies of the [111] gap, however, means that the structure still can be considered periodic-on-average allowing to determine the position of the center of the gap along given direction of propagation.

IV. REFLECTION AND TRANSMISSION ALONG DIRECTIONS OTHER THAN [111]

The most simple method used frequently to probe the band structure of photonic crystals is transmission and/or reflection as a function of the angle of incidence to a [111] surface of the sample [4,8–14,16,17,27]. It should be commented however that along with the problem of the inhomogeneous broadening, which constitutes a general factor complicating such measurements, the conclusions drawn from such experiments are inevitably limited in their scope by several other factors specific for the geometry of oblique incidence [5,48,49].

First is the refraction at the crystal surface [48]. Figure 2(b) displays a set of transmission spectra measured at oblique incidence to (111) oriented piece of the sample GR. It can be seen that the changes of the incidence direction off [111] results in a substantial blueshift and broadening of the stopband. The spectrum 5 in Fig. 2(b) corresponds to the angle 54° off normal to [111] direction, which corresponds to a wave vector changing in the Γ-*X* direction of the fcc BZ. In the vicinity of band edges, however, the normal component of the wave vector is unknown, that implies the uncertainty in the value of the angle of refraction and, correpondingly, the direction in the BZ. Thus the band edges, defined from experimental transmission spectra as the frequencies where the transmission suddenly drops down and then rises up again, do not necessarily fall at the same cross-section of the photonic BZ.

Secondly, recent theoretical calculations for fcc colloidal crystals [49] have shown that there exists another factor, which makes such measurements questionable. It has been shown that several bands are excited under oblique angles and, therefore, the attenuation is defined by contribution from several imaginary wavevectors corresponding to different directions in the BZ. Although the resulting transmission curve does exhibit a well pronounced dip, the edges of the latter, however, have no longer represent the eigenfrequencies of the bands. Thus neither the direction in the BZ, nor the band edges can be uniquely derived from measurements of transmission (reflection) under oblique incidence [50]. At most such measurements can be used for qualitative estimation of the amount of phase space where the stop bands for different directions *do not* overlap. For example, it can be seen from Fig. 2(b) that the sample become transparent for wavelengths around 520 nm when the angle of incidence become larger than 54°.

To avoid these difficulties we used the advantages offered by normal incidence geometry. This method, proposed by us recently [5], requires a set of samples with differently oriented base planes. Under normal incidence the edges of the stopband in transmission (reflection) spectra correspond to

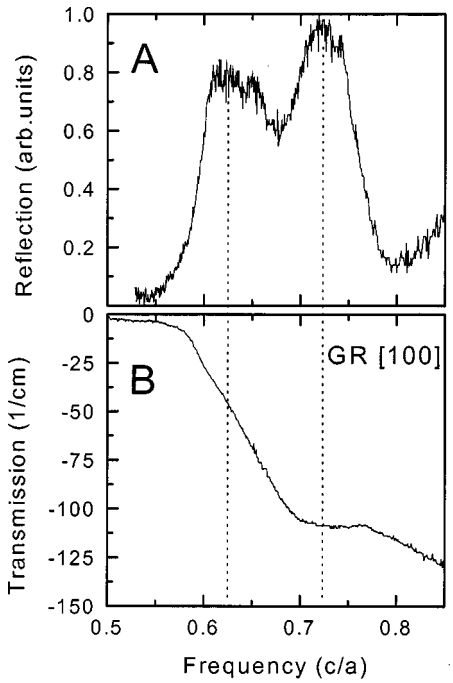

FIG. 4. Reflection (a) and transmission (b) spectra of the [100]-oriented piece of the sample GR immersed in glycerin ($n_b=1.47$). The attenuation is corrected for Rayleigh scattering. Frequency is plotted in normalized units of c/a, where c is a speed of light, a is a lattice constant.

one and the same direction in the BZ. In order to study the photonic band structure we used the different pieces of the samples GR and BL oriented using SEM and TEM, which were sawed along different crystallographic directions. Then, under normal incidence to a given facet, the orientation of the corresponding facet plane of the sample uniquely fixes the direction of the wave vector.

A. [100] direction

The (100) oriented pieces were sawed out from the main samples under the angle of 54° to their $\langle 111\rangle$ growth axis according to data derived from TEM and SEM images. Figure 4 represents transmission and reflection spectra taken at normal incidence to (100) oriented piece of the sample GR with $n_b=1.475$. Under normal incidence to (100) plane the wave vector direction is fixed to the Γ-X direction in a fcc BZ. Since the point L is the nearest to the center of a fcc BZ, therefore the spectral position of the X-photonic gap should correspond to the frequency higher than L-photonic gap. The calculations of the photonic band structure near the point X give position of the gap center as $\nu=0.74$ for the same set of parameters used previously. Indeed in transmission spectrum in Fig. 4(b) the relatively small and very broad drop can be seen with a minimum blueshifted with respect to the [111] gap to $\nu=0.72-0.73$. Therefore it can be supposed that this minimum in transmission is defined mainly by Bragg scattering off (100) parallel planes.

Reflection spectrum presented in Fig. 4(a) displays double peak structure with high-frequency peak position at $\nu=0.73$ roughly the same as the minimum in transmission. This confirms the assignment of the minimum in transmission spectrum at $\nu=0.73$ to Bragg scattering off the (100) fcc planes. The attenuation length at the minimum of the [100] gap can be estimated as 120 cm^{-1}. Such relatively small attenuation with respect to that measured for the [111] gap can be explained by smaller diffraction efficiency of (100) planes. However, the width of the drop estimated from Fig. 4(b) as 16% of its central frequency is at least twice larger than the width of the [111] gap and the transmission signal is worse recovered at high-frequency edge of the [100] drop. The calculations showed that the width of the [100] gap should be much smaller than [111] and for parameters of the sample under consideration should not exceed 0.5% value [23].

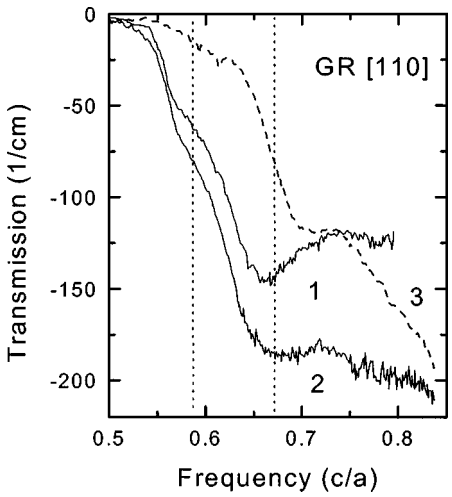

FIG. 5. Transmission spectra of the [110]-oriented piece of the sample GR. Spectra 1 and 2 were measured from the sample immersed in glycerin ($n_b=1.47$) for polarizations $E\|\langle 100\rangle$ and $E\|\langle 110\rangle$, correspondingly. Spectrum 3 corresponds to $n_b=1.33$. The attenuation is corrected for Rayleigh scattering. Frequency is plotted in normalized units of c/a, where c is a speed of light, a is a lattice constant.

These observations give evidence for much higher concentration of lattice defects along $\langle 100\rangle$ direction in comparison with that along the $\langle 111\rangle$, which are responsible for large broadening of the [100] gap. Assuming that [100]-oriented sample was sawed along the direction other than the direction of growth it can be supposed that these are stacking faults parallel to (111) planes, which are responsible for observed behavior. Below we will address this question and will show that appearance of additional peak in reflection can also be explained by contribution from plane stacking faults.

B. [110] direction

The [110]-oriented pieces were sawed by a diamond wheel saw from the main samples GR and BL with their base plane parallel to the $\langle 111\rangle$ growth axis. Under normal incidence to a (110) plane the wavevector is changed in Γ-K direction in a fcc BZ. Spectrum 3 in Fig. 5 represents transmission spectrum taken at normal incidence to the [110]-oriented piece of the sample GR for $n_b=1.33$. Spectrum exhibit a very broad drop with a minimum located at frequency $\nu=0.71$ higher than the [111] gap, as expected. The attenuation at the center of this drop can be estimated as 140 cm^{-1}. Increase of the refractive index of the pores to $n_b=1.475$ (see transmission spectra 1 and 2 in Fig. 5, measured at different polarizations of incident light) results in a redshift of high-frequency drop to $\nu=0.67$ and in increase of attenua-

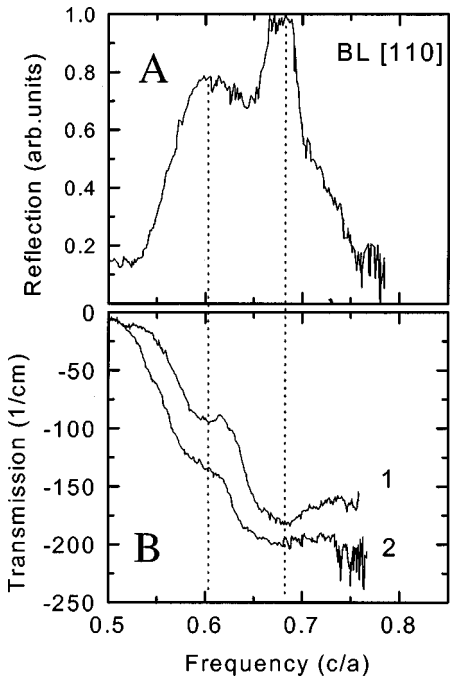

FIG. 6. Transmission spectra of the [110]-oriented piece of the sample BL. Spectra 1 and 2 were measured from the sample immersed in glycerin ($n_b=1.47$) for polarizations $E\|\langle 100\rangle$ and $E\|\langle 110\rangle$, correspondingly. The attenuation is corrected for Rayleigh scattering. Frequency is plotted in normalized units of c/a, where c is a speed of light, a is a lattice constant.

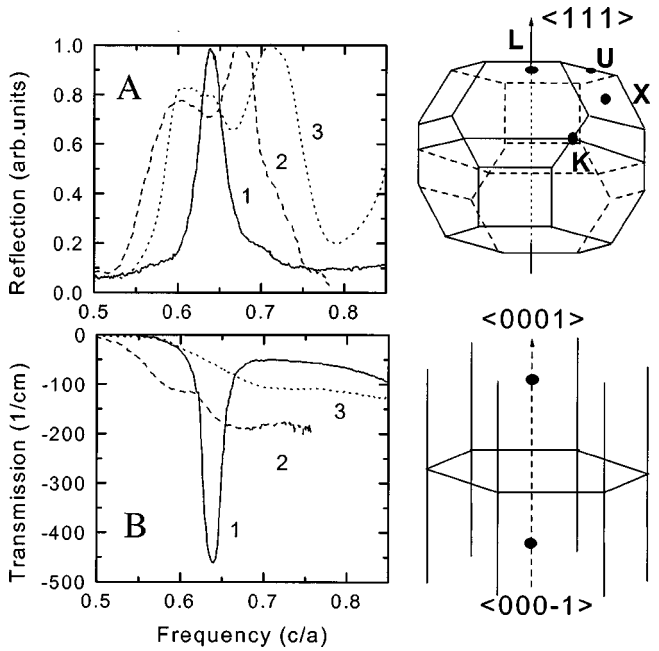

FIG. 7. Reflection (a) and transmission (b) spectra of the sample GR immersed in glycerin ($n_b=1.47$) measured on [111]-, [110]-, and [100]-oriented samples (spectra 1, 2, and 3, correspondingly). Inset shows the fcc first BZ (top) and BZ of randomly close-packed crystal (bottom). Frequency is plotted in normalized units of c/a, where c is a speed of light, a is a lattice constant.

tion at its center to 160–180 cm^{-1}—behavior analogous to that found for the [111] gap. According to full-vector 3D calculations [23] of photonic band structure of fcc lattice with analogous parameters as studied here, the width of the K gap should indeed be larger and, correspondingly, the gap should be deeper than the X gap. Comparison of the corresponding data indeed reveals increased efficiency of Bragg scattering along [110] direction with respect to [100] (compare attenuation of 180 cm^{-1} for the [110] gap with 120 cm^{-1} for the [100] gap). In view of above the high-frequency drop in transmission spectra at $\nu=0.67$ can be attributed to Bragg scattering on the main period along the $\langle 110\rangle$ direction defined by the interplanar distance between (110) fcc planes D_{110} (for BL sample $D_{110}=204$ nm and for GR $D_{110}=252$ nm).

Although these observations allow to ascribe the observed drop in transmission to the [110] gap of fcc structure, the spectra, however, resemble the same broadened shape as that observed for the [100] gap. The width of the [110] gap is, indeed, too broad to be explained only by coherent scattering on a periodic lattice (the width about 1% is expected [23]). The doublet structure analogous to that observed in reflection spectra for [100] orientation can be clearly seen also in transmission spectra of the [110]-oriented sample. Additional shoulder appears at lower frequencies about $\nu=0.59$ with a sizable attenuation nearly twice as small as for the high frequency main drop.

The similar doublet structure appears also in transmission spectra measured at normal incidence to the [110]-oriented piece of BL sample. The high-frequency drop at $\nu=0.68$ and the low-frequency shoulder at $\nu=0.60$ with values of attenuation comparable to that of GR sample can be seen in spectra 1 and 2 on Fig. 6(b), measured for different polarizations. This similarity in spectra of the samples that were synthesized in different runs, possess different lattice constant and different refractive indices, reveals the inherent features in photonic band structure intrinsic to opal photonic crystal.

Similar doublet structure was also observed in reflection spectra measured on both BL and GR [110]-oriented samples. Reflection spectrum on Fig. 6(a) was measured at nearly normal incidence to (110) plane of BL sample for $n_b=1.475$. It displays double peak structure with peaks positions centered roughly at the same frequencies as the high- and low-frequency drops in corresponding transmission spectra 1 and 2 in Fig. 6(b). Therefore, not only the high-frequency drops, but also the low-frequency ones in transmission spectra of (110) oriented pieces of both samples are defined mainly by Bragg scattering. Note that the low-frequency less pronounced feature is centered at surprisingly low frequencies $\nu=0.60$ (sample BL) and $\nu=0.59$ (sample GR), even lower than the positions of the corresponding [111] gaps. Thus these features correspond to scattering off another periodic scale l with relative interplane distance $D_{111}/l\approx 0.9$ (compare the values 0.60/0.523 for sample BL and 0.59/0.64 for sample GR).

In apart from L and X photonic gaps the K-photonic gap is expected to possess considerable polarization anisotropy, since the symmetry of fcc lattice along [110] direction is lower. Polarization dependence was measured for polarizations $E\|\langle 100\rangle$ [see spectra 1 in Figs. 5 and 6(b)] and for $E\|\langle 110\rangle$ [see spectra 2 in Figs. 5 and 6(b)] for both samples BL and GR. The absence of any polarization dependence of the position of the [110] gap can be clearly seen. Note that the [100] gap does not also exhibit any substantial polarization dependence.

Figure 7 summarizes reflection [Fig. 7(a)] and transmission [Fig. 7(b)] spectra of the sample GR for all the directions studied. This final graph is quite surprising since it shows that for some frequency range $0.62<\nu<0.66$ the reflectivity due to Bragg diffraction remains very high irrespective of the propagation direction and polarizations—the usual definition of a complete three-dimensional photonic band gap. It is a well-established theoretical result, however, that the omnidirectional PBG is absent between the lower-frequency bands in fcc photonic crystals with spherical atoms [20–23] for any refractive index contrast.

We explain these results by the presence of disorder in opal samples. In particular our experimental observations presented above give unambiguous evidence for larger disordering in the plane of growth and much smaller along the [111] direction of growth. It is known that usually the stacking anomalies have occurred along only one of the three possible [111] stacking directions, which is in agreement with one-dimensional growth model [43]. It is just this [111] direction, which is known *a priori* and is used in all the experiments published to date [4–14]. Thus these are the plane stacking faults generated in direction perpendicular to [111] direction of growth of colloidal crystal, which are the natural candidates for the explanation of observed behavior. This structural disorder along the (111) planes can also be responsible for the intermixing of photonic bands of different polarizations thus leading to smearing out the polarization dependence. For the fcc crystal with plane stacking faults the interplane distance for [111] direction of growth remains the same for both hcp and fcc phases thus leading to well defined [111] photonic gap. The interplane distance between planes in the direction perpendicular to the [111] growth direction can vary significantly, which can explain the larger broadening of the [110] gap. This model can also explain the appearance of the low-frequency shoulder in the transmission spectra located at frequencies 0.94 times *smaller* than the [111] gap. If we assume that these are (10-10) planes in a hcp structure, which contribute to diffraction at these frequencies, then the ratio between the position of the [10-10]-gap, given by $\nu_{10-10}\sim d\sqrt{3}/2$, and that of the [111], given by $\nu_{111}\sim d\sqrt{2}/\sqrt{3}$, is $\nu_{111}/\nu_{10-10}=0.94$. The latter is indeed very close to the ratio 0.92–0.96 observed experimentally in both of the samples.

V. STUDIES OF DIFFRACTION PATTERNS

The usual method used for determination of the defect structure of the conventional solids is the x-ray diffraction. By analogy the light scattering was successfully used for direct determination of the defect structure in faulted colloidal crystals [15,31,33,34]. It is well known [51] that the reciprocal lattice for randomly hexagonal close-packed structure consists of a hexagonally arranged infinite rods passing through the points $hki0$ and parallel to the [111]-growth direction. The part which is accessible to light is restricted to these rods and the two points at 0001 and $000-1$ as shown in the inset of Fig. 7. The former give origin for streaks, in which the incident white light is dispersed into the spectrum with the longest wavelength at the center of the streak [15]. The latter give two well-defined spots, or poles—the Bragg diffraction off close-packed (111) planes common to both perfect fcc and perfect hcp structures. Thus the pattern of the light diffraction is very sensitive to the concentration of defects and especially stacking faults. For example the dominance of streaks rather than spots in diffraction pattern obtained on colloidal crystal gave evidence for preference of the rhcp structure formation under microgravity conditions [33].

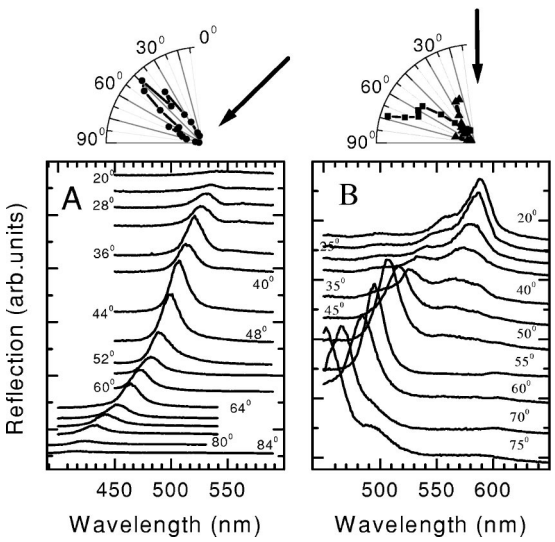

FIG. 8. Diffraction spectra of the sample GR measured as discussed in the text from [111]-oriented (a) and [110]-oriented (b) pieces immersed in glycerin. Angle of incidence is fixed to 45° and to normal incidence on a base plane for (a) and (b), correspondingly. Insets represent radial distribution of the scattered intensity for separate lines in the spectra. Arrow shows the direction of incidence. Angles are not corrected for the refraction.

We studied the diffraction patterns on the [111]- and [110]-oriented pieces of the sample GR. To make measurements the samples were placed on the axis of a cylindrical glass cell (diameter about 3 cm) filled with glycerin ($n_b=1.475$). The cylindrical screen around the cell was used to visualize spatial distribution of the scattered light. The collimated incident white-light beam was produced by incandescent lamp with collimated optics used previously in transmission and reflection experiments. The scattered light was collected using a small aperture lens (less than 1° solid angle). The small diaphragm placed before the lens, the lens itself, and the slit of monochromator, on which the scattered light was focused, formed the collection axis. In some of the experiments the scattered light was also focused in an optical fiber. To study the angle distribution of the intensity of scattered light the orientation of the collection axis was changed gradually along chosen direction allowing to scan angles from 20° to 85° with respect to the incidence beam.

A. Diffraction off (111) planes

Figure 8(a) represents a set of spectra of the light scattered off the [111]-oriented piece of the sample GR. In apart from transmission experiments discussed above [see Fig. 2(b)], where the orientation of the sample with respect to the incidence beam was changed, in diffraction experiments both the orientation of the sample and the angle of incidence were fixed to form 45° off normal to (111) plane. It is the orientation of the collection axis with respect to the normal to

(111) sample plane, which was gradually changed and the spectra of the scattered light were recorded as a function of the angle Θ between collection axis and the [111] axis of the sample. The plane of incidence thus formed is the same used in transmission experiments of Fig. 2(b).

A single bright colored spot diffracted at specular angles dominated the diffraction pattern. It corresponds to Bragg diffraction off (111) planes. The spectrum of the spot at the angle $\Theta = 45°$ consists of a single line centered at 507 nm, that corresponds well to the position of the dip in transmission spectrum 4 of Fig. 2 measured with the same sample orientation. This spot is superimposed on less intense diffusely scattered light. Figure 8(a) shows that even for collection angles far from the specular reflection the diffusely scattered light is also colored. The single line can be found in the spectra, which changes its position from the longest wavelength at smaller Θ to the shortest for larger. The polar plot in the inset of Fig. 8(a) represents the peak intensity of this line as a function of the angle Θ. Its intensity decreases rapidly with changing of the orientation of the collection axis to both larger and smaller Θ with the largest at the angles around 45° corresponding to the specular reflection. Such pattern can be well explained by combination of two scattering channels—coherent diffraction of incident beam off (111) planes and scattering of a diffuse light, analogous to bright Kossel rings usually observed in colloidal crystals for monochromatic illumination [8,2]. A diverging source of white light, necessary to form Kossel rings, is produced when the incident beam is scattered from numerous defects of opal photonic lattice. The scattering of this light on (111) planes is, however, strongly anisotropic since Bragg conditions are satisfied at different angles and for different wavelengths. This anisotropic Bragg scattering of diffuse light can explain the well-defined color seen in the spectra of Fig. 8(a) at the scattering angles Θ far from specular angles.

B. Diffraction perpendicular to the [111] growth direction

For qualitative measurements of the diffraction pattern perpendicular to the growth direction we used white light beam incident normal on [110]-oriented piece of the sample GR. Observation of the distribution of intensity of scattered light on the cylindrical screen reveal diffraction pattern strikingly different from that for [111]-oriented sample. Instead of a single colored pole typical for [111] orientation the fuzzy concentric rings of varying color was observed with a maximum wavelength at the center and shortest at the perimeter. Such ringlike pattern with nearly spherical symmetry also differed strongly from a streaklike pattern usually observed in heavily faulted colloidal crystals [33] and natural opals [15]. These observations allow to suggest that the concentration of stacking faults in our sample is not very large and diffraction pattern, in analogy to interpretation of a diffraction off [111] planes, is dominated by Kossel-like scattering superposed on a system of broadened Bragg spots.

The results of more detailed study of angle and spectral intensity distribution are presented in Fig. 8(b). As for the Fig. 8(a) the orientation of the sample inside the cell was fixed and spectra were measured as a function of the scattering angle Θ between the collection axis and normal to the (110) base surface of the sample. The angle scan was performed along the [111] direction. It can be seen that at most angles spectra exhibit double-peak structure. Increase of the scattering angle Θ results in the blueshift of both peaks. The spectral shift is accompanied by the strong redistribution of the intensity between the doublet in favor of the short-wavelength peak. Polar plot on the inset of Fig. 8(b) represents the intensity of both lines as a function of the scattering angle. In consistence with interpretation of transmission data of Fig. 7 the long-wavelength peak can be attributed to diffraction from a hexagonally ordered domains, while the short-wavelength one is originated from purely fcc packed regions. Indeed in the nearly backward direction [see spectrum at 20° in Fig. 8(b)], where the long-wavelength peak dominates, it is centered at 590 nm ($\nu \approx 0.60$), the value corresponding well to that in Fig. 5. Short-wavelength peak dominates at larger angles, where it is centered around 510 nm ($\nu = 0.70$), close to that observed in experiments in Fig. 5.

This interpretation is consistent with the Kossel-ring pattern expected for diffraction off [110] planes of fcc structure superposed on that off hexagonally ordered [10-10] planes. Indeed, the [110] fcc surface should produce four Kossel rings [pairs of (002) and (111) type] located at the corners of a rectangle [2,8]. Such broadened by disorder rings can mimic nearly spherical symmetry of the observed diffraction pattern. Random hexagonally close-packed layers (as well as pure hcp) are responsible for the maximum in the backward direction [15,2]. This can explain qualitatively different angular distributions of both lines seen in Fig. 8(b).

VI. CONCLUSION

Based on optical and electron microscopy characterization we can conclude that the as-grown chunks of synthetic opals are strongly disordered. The most common type of structural defects are the plane stacking faults concentrated in planes perpendicular to the direction of growth. Although there concentration is usually very high, there are areas virtually free from them. Such areas can be described as mostly fcc single crystals with α up to 0.8–0.9 and sizes up to several thousands of unit cells. Careful selection of the samples allow us to study optical properties on nearly single crystal samples.

We have studied the influence of various types of defects of photonic lattice on photonic band structure of synthetic opals by means of optical transmission, reflection and diffraction. We found that stacking faults are responsible for large broadening and a doubletlike structure of the stop bands along directions other than [111] direction of growth. As a result the inhomogeneously broadened stop bands for different directions and polarizations are overlapped over considerable range of frequencies. This effect, however, does not result in diminished photonic DOS as in the case of an omnidirectional photonic band gap, but rather in a spatial confinement of light in a large volumes of the crystal [46]. The structure, however, can be regarded as fcc, which results in a well-defined fcc related stop bands in the transmission or reflection and corresponding Kossel-ring-like pattern in diffraction. This allow us to extract the information on intrinsic photonic band structure of the fcc structure.

ACKNOWLEDGMENT

This work was supported in part by the RFBR through Grant No. 99-02-18284.

[1] For a review see articles in *Photonic Band Gap Materials*, edited by C.M. Soukoulis, Vol. 315 of NATO Advanced studies Institute, Ser. E (Kluwer, Dordrecht, 1996).
[2] P.A. Rundquist, P. Photinos, S. Jagannathan, and S.A. Asher, J. Chem. Phys. **91**, 4932 (1989); R.J. Carlson, and S.A. Asher, Appl. Spectrosc. **38**, 297 (1984).
[3] J. Martorell and N.M. Lawandy, Phys. Rev. Lett. **65**, 1877 (1990); **66**, 887 (1991).
[4] V.N. Astratov, V.N. Bogomolov, A.A. Kaplyanskii, A.V. Prokofiev, L.A. Samoilovich, S.M. Samoilovich, and Yu.A. Vlasov, Nuovo Cimento D **17**, 1349 (1995).
[5] V.N. Astratov, Yu.A. Vlasov, O.Z. Karimov, A.A. Kaplyanskii, Yu.G. Musikhin, N.A. Bert, V.N. Bogomolov, and A.V. Prokofiev, Phys. Lett. A **222**, 349 (1996).
[6] W.L. Vos, R. Sprik, A. van Blaaderen, A. Imhof, A. Lagendijk, and G.H. Wegdam, Phys. Rev. B **53**, 16 231 (1996); W.L. Vos, M. Megens, C.M. van Kats, and P. Bösecke, J. Phys.: Condens. Matter **8**, 9503 (1996).
[7] Yu.A. Vlasov, V.N. Astratov, O.Z. Karimov, A.A. Kaplyanskii, V.N. Bogomolov, and A.V. Prokofiev, Phys. Rev. B **55**, 13 357 (1997).
[8] I. Tarhan and G.H. Watson, Phys. Rev. Lett. **76**, 315 (1996).
[9] H. Miguez, C. Lopez, F. Meseguer, A. Blanco, L. Vazquez, R. Mayoral, M. Ocana, V. Fornes, and A. Mifsud, Appl. Phys. Lett. **71**, 1148 (1997).
[10] S.G Romanov, N.P. Johnson, A.V. Fokin, V.Y. Butko, and C.M. Sotomayor Torres, Appl. Phys. Lett. **70**, 2091 (1997).
[11] V.N. Bogomolov, S.V. Gaponenko, I.N. Germanenko, A.M. Kapitonov, E.P. Petrov, N.V. Gaponenko, A.V. Prokofiev, A.N. Ponyavina, N.I. Silvanovich, and S.M. Samoilovich, Phys. Rev. E **55**, 7619 (1997).
[12] D. Mei, H. Liu, B. Cheng, Z. Li, and D. Zhang, Phys. Rev. B **58**, 35 (1998).
[13] K. Fukuda, H. Sun, S. Matsuo, and H. Misawa, Jpn. J. Appl. Phys. **37**, L508 (1998).
[14] T. Yamasaki and T. Tsutsui, Appl. Phys. Lett. **72**, 1957 (1998).
[15] J.V. Sanders, Nature (London) **204**, 1151 (1964); **204**, 990 (1964); **209**, 13 (1966); Acta Crystallogr., Sect. A: Cryst. Phys., Diffr., Theor. Gen. Crystallogr. **24**, 427 (1968).
[16] S.G. Romanov, A.V. Fokin, V.I. Alperovich, N.P. Johnson, and R.M. De La Rue, Phys. Status Solidi A **164**, 169 (1997).
[17] H. Miguez, A. Blanco, F. Meseguer, C. Lopez, H.M. Yates, M.E. Pemble, V. Fornes, and A. Mifsud, Phys. Rev. B **59**, 1563 (1999).
[18] A.D. Dinsmore, Y. Tian, and B.R. Ratna (unpublished).
[19] H. Miguez, F. Meseguer, C. Lopez, A. Blanco, J.S. Moya, J. Requena, A. Mifsud, and V. Fornes, Adv. Mater. **10**, 480 (1998); H. Miguez, *et al.* Langmuir **13**, 6009 (1997).
[20] K.M. Ho, C.T. Chan, and C.M. Soukoulis, Phys. Rev. Lett. **65**, 3152 (1990).
[21] H.S. Sözuer, J.W. Haus, and R. Inguva, Phys. Rev. B **45**, 13 962 (1992); H.S. Sözuer, and J.W. Haus, J. Opt. Soc. Am. B **10**, 296 (1993).
[22] K. Busch and S. John, Phys. Rev. E **58**, 3896 (1998).
[23] A. Moroz and C. Sommers, J. Phys.: Condens. Matter **11**, 997 (1999); A. Reynolds *et al.*, Phys. Rev. B **60**, 11 422 (1999).
[24] J. Wijnhoven and W.L. Vos, Science **281**, 802 (1998).
[25] A.A. Zakhidov, R.H. Baughman, Z. Iqbal, C. Cui, I. Khairulin, S.O. Dantas, J. Marti, and V.G. Ralchenko, Science **282**, 897 (1998).
[26] Yu.A. Vlasov, N. Yao, and D.J. Norris, Adv. Mater. **11**, 165 (1999).
[27] S.Y. Lin, J.G. Fleming, D.L. Hetherington, B.K. Smith, R. Biswas, K.M. Ho, M.M. Sigalas, W. Zubrzycki, and S.R. Kurtz, Nature (London) **394**, 251 (1998).
[28] L.V. Woodcock, Nature (London) **385**, 141 (1997); **388**, 236 (1997); P.G. Bolhius, D. Frenkel, S.C. Mau, and D.A. Huse, **388**, 235 (1997).
[29] S.-C. Mau and D.A. Huse, Phys. Rev. E **59**, 4396 (1999).
[30] A.D. Bruce, N.B. Wilding, and G.J. Ackland, Phys. Rev. Lett. **79**, 3002 (1997).
[31] H. Versmold, Phys. Rev. Lett. **75**, 763 (1995); C. Dux and H. Versmold, *ibid.* **78**, 1811 (1997).
[32] N.A. Verhaegh, J.S. van Duijneveldt, A. van Blaaderen, and H.N.W. Lekkerkerker, J. Chem. Phys. **102**, 1416 (1995);
[33] J. Zhu, M. Li, R. Rogers, W. Meyer, R.H. Ottewill, STS-73 Space Shuttle Crew, W.B. Russel, and P.M. Chaikin, Nature (London) **387**, 883 (1997).
[34] P.N. Pusey, W. van Megen, P. Bartlett, B.J. Ackerson, J.G. Rarity, and S.M. Underwood, Phys. Rev. Lett. **63**, 2753 (1989).
[35] S. Pronk and D. Frenkel, J. Chem. Phys. **110**, 4589 (1999).
[36] H.J. Queisser and E.H. Haller, Science **281**, 945 (1998).
[37] Yu.A. Vlasov, M. Deutsch, and D. J. Norris, Appl. Phys. Lett. **76**, 1627 (2000).
[38] L. Samoilovich and M. Samoilovich, Research Institute for the Synthesis of Minerals, Alexandrov, Russia.
[39] N.D. Deniskina, D. V. Kalinin, and L.V. Kazantseva, *Precious Opals, Their Synthesis and Natural Genesis* (Nauka, Novosibirsk, 1988) p. 353.
[40] W. Stöber, A. Fink, and E. Bohn, J. Colloid Interface Sci. **26**, 62 (1968).
[41] P.N. Pusey, and W. van Megen, Nature (London) **320**, 340 (1986); Phys. Rev. Lett. **59**, 2083 (1987).
[42] R.C. Salvarezza, L. Vazquez, H. Miguez, R. Mayoral, C. Lopez, and F. Meseguer, Phys. Rev. Lett. **77**, 4572 (1996).
[43] K.E. Davis, W.B. Russel, and W.J. Glantsching, Science **245**, 507 (1989).
[44] E.A. Monroe, D.B. Sass, and S.H. Cole, Acta Crystallogr., Sect. A: Cryst. Phys., Diffr., Theor. Gen. Crystallogr. **25**, 578 (1969).
[45] M.S. Elliot, B.T.F. Bristol, and W.C.K. Poon, Physica A **235**, 216 (1997).
[46] Yu.A. Vlasov, M.A. Kaliteevski, and V.V. Nikolaev, Phys. Rev. B **60**, 1555 (1999).
[47] K.W.-K. Shung and Y.C. Tsai, Phys. Rev. B **48**, 11 265 (1993).
[48] E. Yablonovitch, and T.J. Gmitter, Phys. Rev. Lett. **63**, 1950 (1989).
[49] V. Yannopapas, N. Stefanou, and A. Modinos, J. Phys.: Condens. Matter **9**, 10 261 (1997).
[50] Note, that the abovementioned limitations of this method do not allow to make *positive* conclusion on existence of a complete omnidirectional photonic band gap, which is based solely on observation of the overlapping stopbands for all possible angles of incidence on a given sample plane.
[51] A. Guinier, X-*ray Diffraction* (Freeman, London, 1963).